



## Seismic performance of prefabricated sheathed cold-formed thin-walled steel buildings: Shake table test and numerical analyses

Yu Guan <sup>a</sup>, Xuhong Zhou <sup>a,b,c</sup>, Xinmei Yao <sup>a</sup>, Yu Shi <sup>b,c,\*</sup>

<sup>a</sup> College of Civil Engineering, Chang'an University, Xi'an, Shaanxi, 710061, China

<sup>b</sup> College of Civil Engineering, Chongqing University, Chongqing, 400045, China

<sup>c</sup> Key Laboratory of New Technology for Construction of Cities in Mountain Area (Ministry of Education), Chongqing University, Chongqing, 400045, China



### ARTICLE INFO

#### Article history:

Received 28 June 2019

Received in revised form

21 October 2019

Accepted 23 October 2019

Available online 27 November 2019

#### Keywords:

Prefabricated CFS building

Shake table test

Dynamic characteristic

Seismic behavior

### ABSTRACT

Cold-formed thin-walled steel (CFS) building systems are widely used in residential construction due to their good seismic behaviour, rapid construction efficiency and high material properties. Although significant work has been conducted on CFS members and subsystems, including studs, beams, shear walls and floors, few researches exist on the seismic performance of full-scale building systems. In order to investigate the seismic response of the CFS building system, shake table tests on a prefabricated full-scale one-story complete building were carried out. The fundamental frequency, damping ratio, displacement response and acceleration response were summarized in this paper. Then a simplified nonlinear finite element model was established with commercial software ABAQUS and validated against the test results. It was found that the developed model was suitable to accurately simulate the dynamic responses of the tested building. Hereafter, parametric studies were performed based on the validated model to investigate the influence of key parameters on the seismic behaviour of the CFS systems, including sheathing of shear walls, diagonal brace, numbers of stories, aspect ratio as well as plan layout. Finally, based on the test data and numerical analysis results, improved seismic construction measures were proposed to provide more applicable objectives for CFS structures.

© 2019 Elsevier Ltd. All rights reserved.

## 1. Introduction

It is well known that prefabricated CFS building systems typically comprise of assembled structures including gravity walls, shear walls, floors and roof trusses, fastened together with fasteners or self-tapping screws. These prefabricated structures offer the benefits of manufacturing elements such as walls, floors and roof trusses are all in workshop condition to achieve a high standard of accuracy and rapid construction efficiency. CFS members and structural sheathing panels have been often used in low-rise and mid-rise residential buildings, particularly in high seismic regions, taking advantages of the lightweight structural components, excellent seismic performance, heavy industrialisation, environment protection and good economy. In past years, researches on the seismic behaviour of CFS building systems are mostly focus on the lateral performance of CFS shear walls. Extensive experimental and theoretical researches have been undertaken to explore the effects

of shear wall sheathing properties [1–4], fastener characterization [5], stud spacing [6], wall aspect ratio [7], window and door opening [8], loading pattern [9] as well as hold-downs [10], on the seismic performance of CFS walls. Noritsugu et al. [11] presented the effective strip method to predict the nominal strength of cold-formed steel framed shear wall with steel sheet sheathing without conducting full-scale shear wall tests. The shear stiffness of cold-formed steel wall frame with lightweight concrete was proposed by Hoseinpoor et al. [12] under cyclic loading test. Pourabdollah et al. [13] used gusset plate in the braced to stud connection of the K-braced CFS shear panels, which significantly increasing their shear strength, energy dissipation and ductility capacities under cyclic loading. Furthermore, to reveal a better understanding of the seismic performance of CFS building systems, Sato [14] verified the adequacy of seismic performance factors for Cold-Formed Steel special bolted moment frames, which showed that the proposed seismic performance factors met the acceptance criteria and could provide a sufficient margin against collapse under the maximum considered earthquake. Fiorino and Shakeel et al. [15,16] evaluated a suitable value of behaviour factor of CFS shear walls following the procedures of FEMA P695 through the static pushover and the incremental dynamic analysis, which concluded that a behaviour

\* Corresponding author. College of Civil Engineering, Chongqing University, Chongqing, 400045, China.

E-mail address: [shiyucivil@cqu.edu.cn](mailto:shiyucivil@cqu.edu.cn) (Y. Shi).

factor of 2.0 for the CFS shear walls with gypsum board sheathing and 2.5 for CFS strap-braced stud wall were appropriate.

However, the seismic response of CFS complete building systems is not simply a superposition of shear wall behavior, and the investigations on CFS walls alone are not sufficient for building predictions. The seismic behavior of CFS buildings has only seen limited research. Huang and Su et al. [17,18] carried out a shake table test early on two dimensional framing configurations of a full-scale three-story CFS residential building to characterize the seismic behavior of this structure. The CFS shear wall was built with C-shape studs, U-shape rim tracks, C-shape diagonal bracings, U-shape transverse bracings, oriented strand board (OSB) sheathing as outside structural panel and gypsum board as inside non-structural panel. It was found that hold-downs were essential for the seismic performance of buildings, reliable measures were suggested to be taken for prevention loosening of hold-downs at the bottom and inter stories, and transverse and diagonal bracings showed little contribution to earthquake resistance of structures. Moreover, shake table tests were further conducted by Li et al. [19,20] on two full-scale two-story CFS framed buildings sheathed with OSB and ribbed corrugated steel sheets as shear wall panels respectively to evaluate the earthquake performance of CFS building structures. Authors concluded that the seismic behavior of CFS buildings is governed by the connection performance of self-drilling self-tapping screws fastening the sheathing and CFS frames. Furthermore, in order to access the performance-based seismic design method of CFS structures, three dimensional shake table tests were carried out on two two-story building models in various construction phases by Peterman et al. [21] to investigate the system-level [22] and subsystem-level response [23] of CFS buildings under seismic excitations. Meanwhile, Schafer et al. [24] summarized the shear wall tests, cyclic member and fastener characterization, as well as shake table tests on the whole buildings, which shown significant difference between advanced engineering models of the lateral resistance system and the excellent behavior of the whole building system. In addition, Hutchinson and Wang et al. [25,26] conducted seven earthquake tests, then live fire tests and two post-fire earthquake tests on a full-scale six-story CFS buildings to evaluate the earthquake, post-earthquake fire and post-fire earthquake performance of mid-rise CFS framing buildings. Fiorino et al. [27] studied the dynamic response and seismic performance of CFS buildings by conducting full-scale shake table tests and provided the obtained dynamic identification and earthquake performance. More recently, Ye et al. [28] proposed a simplified analytical model of a novel mid-rise CFS structure system employing the concrete-filled tube column as the end stud, and then conducted a shake table test on a five-story 1: 2 scale CFS composite shear wall building to validate the simplified model. Fiorino et al. [29] performed shake table tests on two reduced-scale (1:3) three-storey two-bay seismic force-resisting systems of cold-formed steel structures with strap-braced walls. The seismic response could be considered as satisfactory, because the system seems to have inherent ductility even without a designated energy dissipating mechanism.

Considering there has been a few laboratory studies on the seismic performance of full-scale CFS building, it is unfortunately that few experimental researches has been conducted for the prefabricated CFS building systems. In addition, the lateral behavior of this CFS shear walls with diagonal braces has been investigated through horizontal low cyclic loading tests by Wang [30], and the results show that the arrangement of diagonal braces result in an effective improvement of the load bearing capacity, stiffness and energy dissipation capacity of walls. As a result, this shear wall with diagonal braces was applied in this prefabricated CFS building systems. To investigate the prefabricated CFS building systems with diagonal braced OSB-sheathed shear walls, an experimental

investigation on the seismic performance of a full-scale one-story CFS building was carried out by Shi [31]. Then a numerical model was developed to simulate the tested building and validated against the shake table test results. The verified model was consequently employed for parametric study to analyze the key influences on the earthquake response of prefabricated CFS building systems. Based on the test data and numerical analysis results, improved design methods were proposed to provide more applicable objectives for CFS structures.

## 2. Shake table test

### 2.1. Building specimen design

A full-scale one-story prefabricated shake table model adopted from the engineering case shown in Fig. 1a were designed in accordance with JGJ 227-2011 [32]. The purpose of this design was to capture the seismic response of prefabricated CFS buildings under earthquake action. This building included CFS-framed, OSB-sheathed shear walls and CFS-framed, OSB-sheathed roof trusses. The plan layout of this building is with the dimension of 1.9 m × 2.9 m, and the total height was 3.62 m with shear walls height of 2.5 m, as shown in Fig. 1b and c. A model base as shown in Fig. 1d was designed to connect CFS building specimen to the shake table plan. The model base built with hot-rolled steel made of Q235B steel grade with a nominal strength of 235 MPa. The hold-downs were arranged at the wall corners and the door and window openings and were screwed to the bottom end of chord stud with sixteen ST5.5 screws. The baseplate of hold-downs and bottom tracks were connected to the model base through M18 hold-down bolts. Moreover, M16 shear bolts were also required to connect the bottom track and model base. The arrangement of these bolts is shown in Fig. 1e. The model base connected to the shake table plan via four connection supports by M22 high-strength bolts.

Four shear walls with doors or windows depicted in Fig. 2 were made of 90 × 50 × 10 × 1.0 mm C-shape studs, 90 × 50 × 1.0 mm U-shape rim tracks, diagonal braces with the same section of studs, and transverse braces with the same section of tracks. Three limbs built-up columns of two 90 × 50 × 10 × 1.0 mm C-shape components combined with one 86 × 46 × 10 × 1.0 mm C-shape components were used to strengthen the openings of four shear walls as shown in Fig. 2e. Three limbs built-up columns of three 90 × 50 × 10 × 1.0 mm C-shape components were used to strengthen the wall corners of L1 and L3 as shown in Fig. 2f. Moreover, double L-headers were employed upon the openings in accordance with AISI S230-15 [33]. For all shear walls, they were sheathed with 9.5 mm thick OSB panels on both sides. Moreover, 15 mm thick anticorrosive wood veneer was connected to the outside of OSB panels. The CFS members in the shear walls were connected using ST4.8 × 19 mm (diameter × length) self-tapping screws, and ST4.2 × 32 mm self-tapping screws were used to connect the OSB panels and CFS members. The spacing of ST4.2 screw was 305 mm on center in the field and 152 mm on center around all edges.

Roof trusses presented in Fig. 3a were made of three kinds of trusses labelled G1, N1 and N2 respectively. For G1 shown in Fig. 3b, the section dimensions of chord members were 70 × 45 × 1.0 mm U-shape components, and it was 70 × 46 × 10 × 1.0 mm C-shape components for the web members. The basic components of roof truss were shown in Fig. 3c. Similarly, for N1 and N2 shown in Fig. 3d, the section dimensions of chord members were 75 × 42 × 12 × 10 × 1.0 mm hat section components, and it was 75 × 42 × 10 × 1.0 mm C-shape components for the web members. Upper longitudinal bracing GF shown in Fig. 3e, were set between the upper chord members of roof truss G1 and N2 to provide support for the roof board extending out of the wall. The section

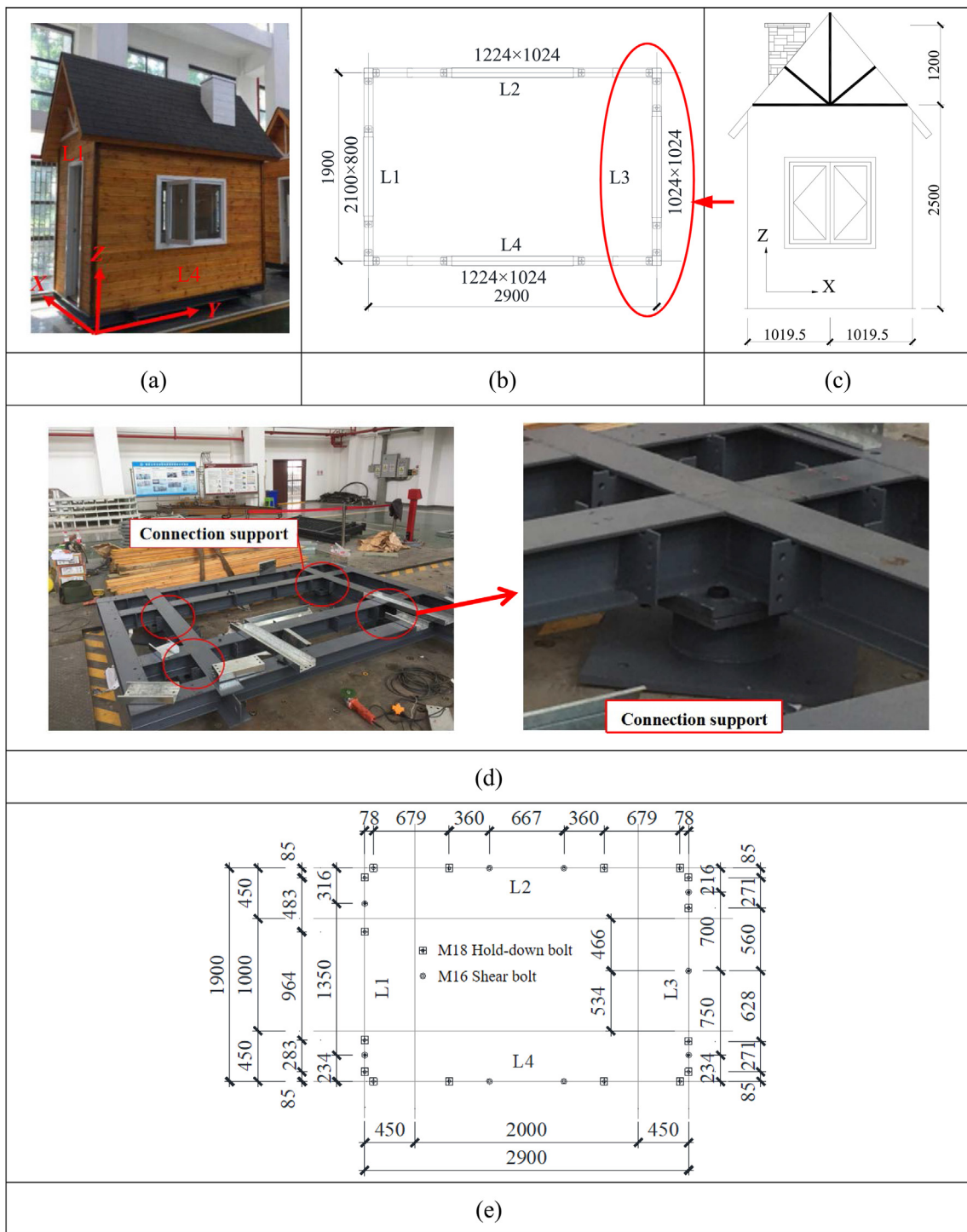


**Fig. 1.** CFS building specimen. (a) Overall view of tested building. (b) Building plan layout. (c) Vertical view of L3. (d) Model base. (e) Layout of hold-down bolts and shear bolts.

dimension of GF was  $70 \times 46 \times 10 \times 1.0$  mm C-shape components. The upper lateral bracings and bottom lateral bracings with  $75 \times 50 \times 10 \times 1.0$  mm C-shape section were put on the top chord and bottom chord of roof trusses respectively, as shown in Fig. 3f. The longitudinal vertical bracings with four  $75 \times 50 \times 10 \times 1.0$  mm C-shape section were put at the middle web member of the roof trusses, as shown in Fig. 3f. The roof trusses were sheathed with 12 mm thick OSB panels. The CFS members in the roof trusses were connected using ST4.8 × 19 mm (diameter × length) self-tapping screws, and ST4.2 × 32 mm self-tapping screws were used to

connect the OSB panels and roof trusses. The spacing of ST4.2 screw was 152 mm on center. Connection fittings were adopted to connect the wall and roof trusses through ST5.5 self-tapping screws as shown in Fig. 3g. The details of connection fitting was shown in Fig. 3h.

The structural members in this building specimen all adopted Q345 steel grade with a nominal strength of 345 MPa. And the material properties of steel members were tested according the Chinese standard GB/T 228.1–2010 [34]. It can be obtained in the material test that the average yield strength and tensile strength of

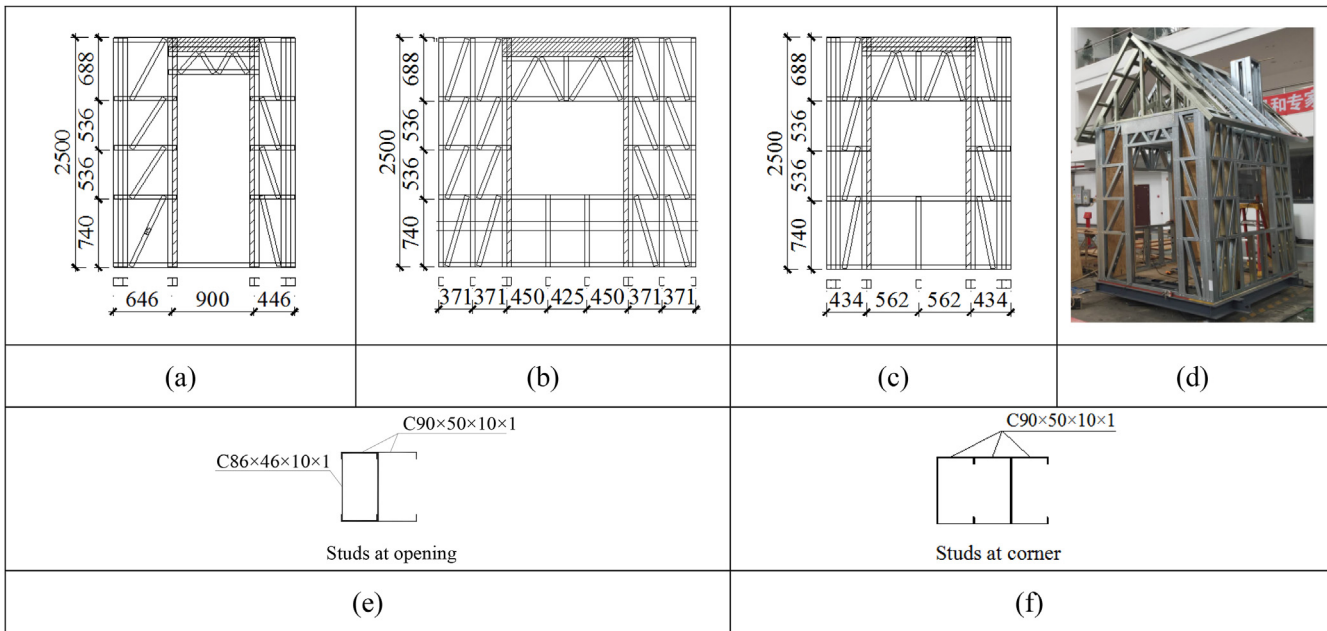


**Fig. 2.** Details of shear walls. (a) Shear wall of specimen L1. (b) Shear wall of specimen L2 (L4). (c) Shear wall of specimen L3. (d) Skeleton of CFS building specimen. (e) Built-up stud at opening position. (f) Built-up stud at corner.

steel were 322.4 MPa and 477.73 MPa, respectively. The average elongation rate after fracture was 30.4%. The elastic modulus and Poisson's ratio were  $2.08 \times 10^5$  MPa and 0.3, respectively. The material property of the OSB sheathing was in accordance with Zhou [35].

In this shake table test of the full-scale one-story prefabricated CFS building, supplemental mass of the specimen was not considered reasonably. Because the construction of this building with decoration design was identify to that in actual engineering case, where walls and the roof were all constructed with insulating layer and water proof layer, the dead load of this model is actual and it is not necessary to add other dead load. Moreover, this model is a single-story CFS building with an inaccessible roof, therefore, the floor live load was not taken into account in the supplemental mass. Furthermore, according to the Chinese standard GB 50009-2012 [36], the snow load of the roof is 0.5 kN/mm<sup>2</sup>, and the combination coefficient of the snow load should be multiplied by 0.5 when the earthquake action is considered. As a result, the additional mass should be about 0.25 kN/mm<sup>2</sup>, while the uniform snow load can be replaced and equivalent to the weight of furniture in the building specimen, which was more consistent with the real case. Consequently, it can be seen that the building specimen can represent the actual situation, and the seismic response was not influenced by the supplemental mass.

## 2.2. Instrumentation and test program

Sixteen accelerometers transducers were arranged for acceleration response measurements on two directions during the dynamic tests, two of which were placed on the shake table to obtain the input accelerations, ten were placed at four corners and the central of the bottom floor, and four were arranged at the both mid span position of the bottom chord members and the top of the end truss, as shown in Fig. 4.

The tested full-scale one-story prefabricated CFS building was designed according to seismic conditions in Chongqing, China. The seismic design intensity was 6, the soil condition was type II, and

the classification of design earthquake was the first group with a characteristic period of 0.35s as specified in the Chinese standard GB 50011-2010 [37]. The design peak ground acceleration (PGA) was 0.05 g for the probability of occurrence equal to 10% in 50 years.

Three ground motion were selected according to GB 50011-2010 [37], including Taft, El Centro, and one Shanghai artificial wave. The time-history curves of seismic acceleration were shown in Fig. 5. The unscaled spectral accelerations and the mean spectra of the three input ground motions are given and compared with the design spectral as depicted in Fig. 6a. The seismic influence coefficient curve of the mean spectra should be close to that of the design spectrum at the fundamental periods of the structure. The CFS building structure was subjected to earthquake ground motions at three intensity levels, including frequent occurring earthquake with a PGA of 0.035 g at intensity level 7° (FOE7), design basis earthquake with a PGA of 0.100 g at intensity level 7° (DBE7) and maximum considered earthquake with a PGA of 0.220 g at intensity level 7° (MCE7), as shown in Table 1. In order to match the peak acceleration of time history analysis at different intensity levels, the spectral accelerations were scaled to represent various intensity levels by matching the peak ground acceleration stipulated in Fig. 6b. During the shake table tests, the structure was loaded bi-directionally, one direction was set as the main direction and the PGA in the other direction was proportioned by a factor of 0.85 [37].

The general loading program is shown in Table 1. Before loading and after each excitation, white noise scanning was applied in order to access the changes of natural frequencies of the CFS building.

## 2.3. Test results and discussion

### 2.3.1. Frequency and damping

To investigate the dynamic properties of the CFS building system, the fundamental frequency and damping ratio of the model in two directions were obtained by the white noise acceleration response tests. Fig. 7 shows changes of fundamental frequencies and damping ratios of this CFS building. It can be seen in Fig. 7a that

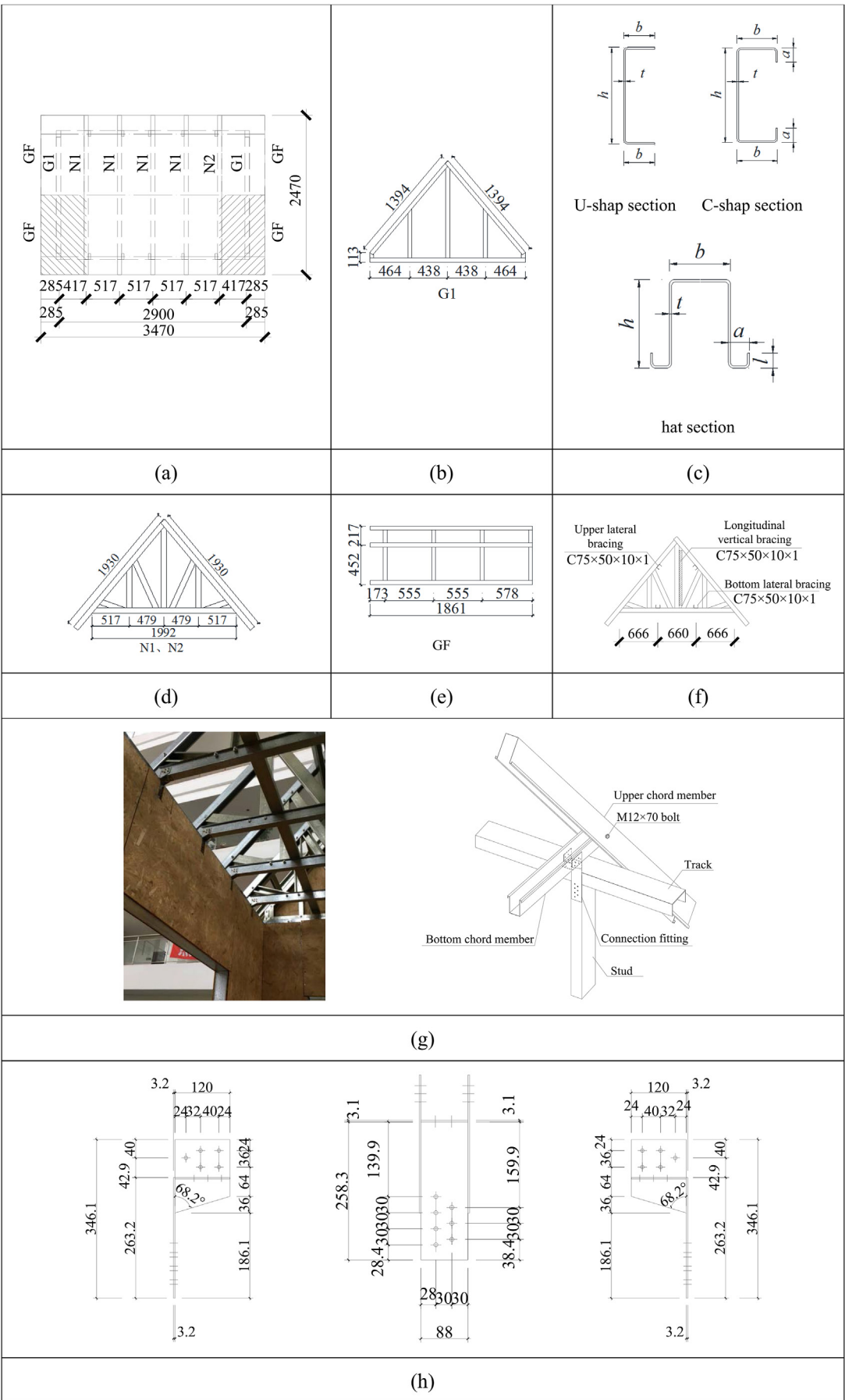


**Fig. 3.** Details of roof trusses. (a) Plane layout. (b) Details of G1. (c) Section size of component. (d) Details of N1 and N2. (e) Details of GF. (f) Roof lateral bracing system. (g) Connection details between roof truss and wall. (h) Details of connection fitting.

the fundamental frequencies were basically identical in the testing program, demonstrating the constant whole stiffness of the CFS building under FOE7, DBE7 and MCE7. It was also consistent with the no observed damage of the whole building, particularly at weakness parts in the structure such as wall panels, headers and openings, as shown in Fig. 8. The measured frequency was slightly higher than the calculated value of formula JGJ 227-2011 [32], which was 9.2–13.7 Hz. The frequency of the CFS structure had been increased due to the addition of inclined bracing in the shear walls, which was more rigid than the CFS structure used ordinary shear walls. Moreover, the frequency in Y direction was higher than that in X direction by up to 52.8%, showing the Y-directional stiffness was stronger than the X-directional stiffness.

In addition, with the intensity of the earthquake motions increased, damping ratio had an upward trend, but the increase was small. The structure had a good seismic performance and higher safety under the action of 7° rare earthquake. The damping ratio of CFS building roughly maintained around 3%, which is consistent with the provisions in the specification JGJ 227-2011 [32]. The damping ratio in Y direction was higher than that in X direction, and this was mainly due to the higher lateral stiffness and better energy dissipation performance of shear walls in Y direction than that in X direction.

### 2.3.2. Acceleration amplification

The acceleration response is often represented by the relationship of the acceleration amplification factor  $\beta$  and the height of the building. The acceleration amplification factor is the ratio of the maximum acceleration of the measuring point and the maximum acceleration of the vibration table ground. Presented in Table 2 and depicted in Fig. 9 are the maximum acceleration and its corresponding acceleration amplification factor under three different earthquake intensity levels. The acceleration at vibration table ground (at 0 m height) was defined as the input earthquake shaking acceleration obtained from MA-X or MA-Y. The acceleration at the bottom of shear walls (at 0.4 m height) in CFS building obtained from M1-5-X or M1-5-Y. The acceleration at lower chord of roof truss (at 2.5 m height) in CFS building obtained from M2-X or M2-Y. Moreover, the acceleration at upper chord of roof truss (at 3.6 m height) in CFS building obtained from M3-X or M3-Y. In Fig. 9, FOE7(X) means the acceleration amplification factors was in X direction of CFS building under FOE7.

It can be known in Table 2 that the acceleration response increased with the height of the building. The acceleration responses in Y direction were generally smaller than those in X direction, which may resulted from the weaker stiffness in X direction of CFS structure. As shown in Fig. 9, the acceleration response of CFS building was the largest under Shanghai artificial wave in FOE7 and DBE7, while the earthquake response of CFS building was the largest under El Centro wave in MCE7. The acceleration response of the CFS building to Taft wave, El Centro wave and Shanghai artificial wave had no obvious regularity under the action of 7° earthquakes, which was related to the spectrum characteristics of seismic waves. Generally speaking, the overall stiffness of the structure degraded as well as the damping ratio increased due to different degrees of structural damage during the earthquake. As a result, the acceleration amplification coefficient at different measuring points would decrease with the increase of input seismic acceleration. However, the CFS building in this paper did not suffer obvious damage under the action of a 7° earthquake, and the damping ratio remained basically unchanged, so the law in CFS building was not significant.

### 2.3.3. Story drift

The displacement history curves of this CFS building can be acquired through quadratic integral to the acceleration history

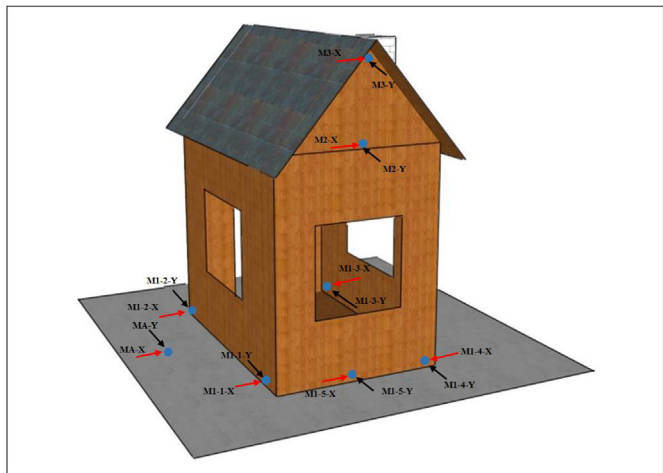
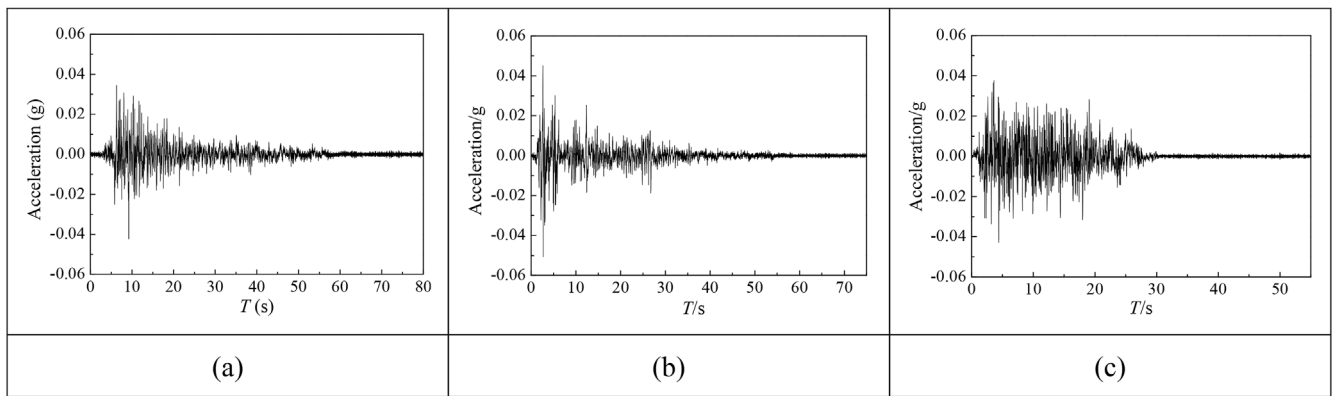


Fig. 4. Arrangement of accelerometers.

curves, and the maximum relative displacement was defined as the maximum difference between each measurement displacement in CFS building and shake table ground displacement. Then the displacement response is reflected by the maximum story drift which is the ratio of the maximum relative displacement and the building height. In order to evaluate the story drift, eight measurements including MA-X, MA-Y, M1-5-X, M1-5-Y, M2-X, M2-Y, M3-X and M3-Y installed at each building height (0 m, 0.4 m, 2.5 m and 3.6 m) to obtain the horizontal displacement in X and Y direction respectively were taken into consideration. Table 3 shows the maximum relative displacements of each measuring point under three different earthquake intensity levels, and Fig. 10 shows the maximum story drifts in X excitation orientation where only the measuring points at the height of 2.5 m and 3.6 m were accounted for. The FOE7(X) in Fig. 10, represents the maximum story drift of CFS building in X direction under FOE7.

It can be known in Table 3 that the maximum displacements increased with the height of CFS building, and the maximum displacements of the structure in X direction were generally greater than that in Y direction, which was also related to the weaker stiffness of CFS building in X direction. Similar to the acceleration response, the displacement response of CFS building was the largest under Shanghai artificial wave in FOE7 and DBE7, while the displacement response of CFS building was the largest under El Centro wave in MCE7, which was related to the spectrum characteristics of seismic waves. Under the action of the same seismic wave and different seismic intensity, the displacements of each measuring point in the CFS structure increased with the increase of input seismic acceleration, indicating that the structural displacement response increased in proportion to the seismic intensity.

As shown in Fig. 10, under the action of the same seismic intensity, the story drift of CFS structure did not increase with the increase of the structural height. The maximum story drift of the structure occurred at the height of 2.5 m, indicating that the weak position of the single-storey CFS building is 2.5 m, which was related to the large difference of lateral stiffness between the shear wall and the roof truss. The maximum story drifts under FOE7, DBE7 and MCE7 were 1/836, 1/402 and 1/186, respectively. For comparison, the maximum design story drift ratio is 2.5% in according to ASCE/SEI 7-16 [38], and it is 1/300 under FOE in technical specification JGJ 227-2011 [32]. In the standard Code GB 50011-2010 [37], the maximum elastic design story drift is 1/250 and the maximum elastic-plastic story drift is 1/50. The maximum story drift ratios for CFS building at excitations consistent with FOE7 and DBE7 levels were both within 1/250 and 1/300, and the maximum



**Fig. 5.** Time-history curves of seismic acceleration. (a) Taft wave. (b) El Centro wave. (c) Shanghai artificial wave.

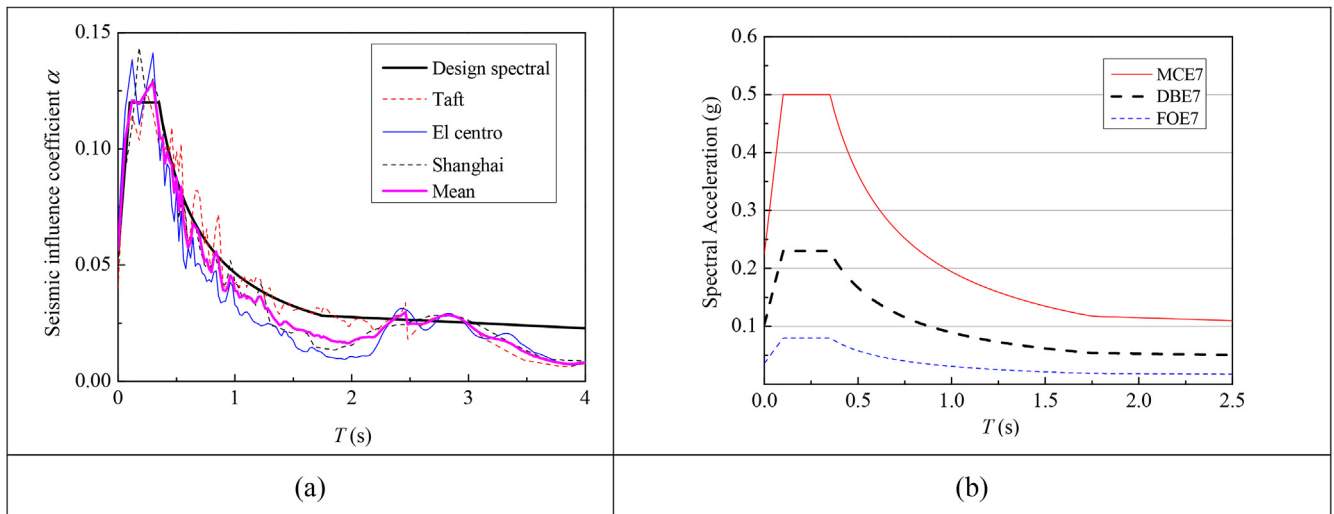


**Fig. 6.** Response spectra. (a) Comparison between spectra of selected ground motions and design spectra. (b) The design spectra for different intensity level.

**Table 1**  
Loading program.

Sequence	Level	Seismic wave	Excitation orientation	PGA/g	
				X	Y
1		White noise		0.050	0.050
2	FOE7	Taft	X	0.035	0.030
3			Y	0.030	0.035
4		El centro	X	0.035	0.030
5			Y	0.030	0.035
6		Shanghai	X	0.035	0.030
7			Y	0.030	0.035
8		White noise		0.050	0.050
9	DBE7	Taft	X	0.100	0.085
10		El centro	X	0.100	0.085
11		Shanghai	X	0.100	0.085
12		White noise		0.050	0.050
13	MCE7	Taft	X	0.220	0.187
14		El centro	X	0.220	0.187
15		Shanghai	X	0.220	0.187
16		White noise		0.050	0.050

story drift ratio under MCE7 was within 2.5% and 1/50. Therefore, the displacement response demonstrated excellent seismic performance of the prefabricated CFS structure to resist 7° earthquakes, and it is stiffer and stronger than engineering design suggest.

### 3. Nonlinear finite element (FE) analysis

#### 3.1. Development and validation of finite element model of the CFS building

In order to ensure the efficiency of the analysis, a nonlinear finite element (FE) model was established by employing the software ABAQUS [39] to evaluate the seismic performance of the full-scale one-story prefabricated CFS building, as shown in Fig. 11. The wall sheathing, roof sheathing and the CFS components including both chord and web members of roof trusses, studs, connection fittings, tracks and bracings of shear walls were simulated by using 4-noded reduced integral shell element S4R. According to experimental phenomena, the self-tapping screw connections between steel components were simulated by using the coupling constraint, in which the displacements along  $x$ ,  $y$ , and  $z$  directions at two nodes of screw locations were constrained, which were the same as the screw connections between CFS members and OSB sheathings. Tie constraints were applied to simulate constrained relationship between the shear wall and shear wall, the shear wall and wall panel, the shear wall and roof truss as well as the roof truss and roof panel. In order to ensure that penetration did not occur among elements in contact, frictional contact was established by using hard contact for normal reaction and coulomb friction model for tangential reaction. Referring to the standard GB50017-2017 [40], the anti-slip coefficient of friction surface was 0.35. As the bottom of CFS

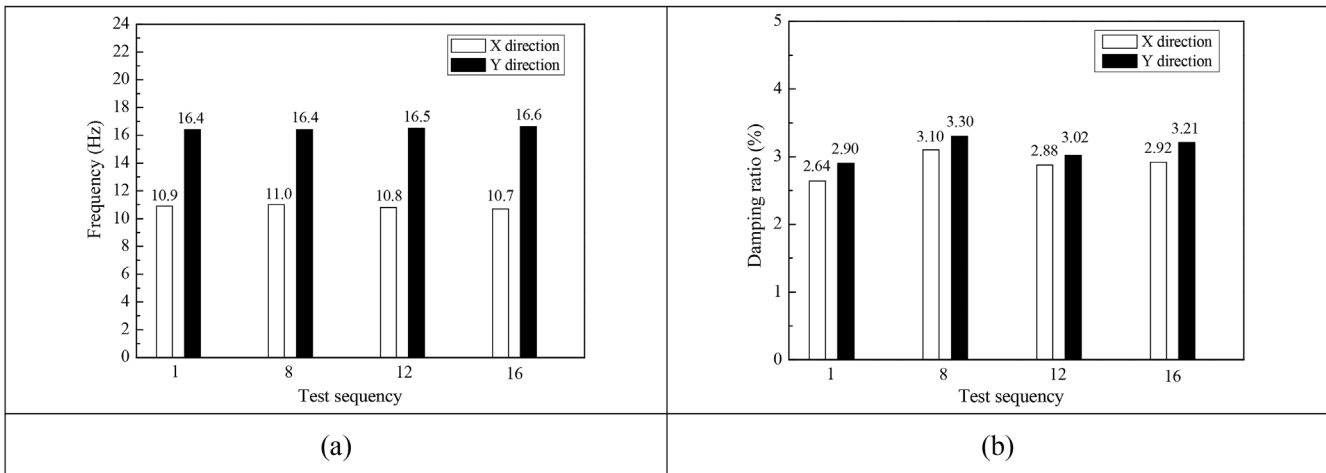


**Fig. 7.** Fundamental frequency and damping ratio. (a) Fundamental frequency. (b) Damping ratio.



**Fig. 8.** Test phenomenon at weakness parts of the structure. (a) Door position. (b) Window position. (c) Edge stud position. (d) Roof position.

**Table 2**

Comparison of maximum accelerations at the location of measurement points between test and FE analysis results (gal).

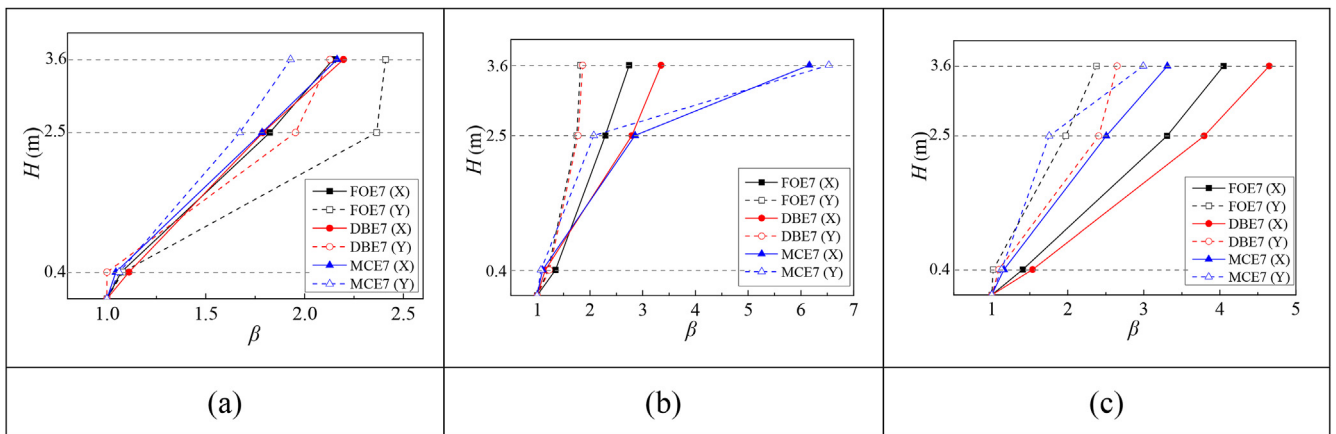


**Fig. 9.** Acceleration amplification factors in X excitation orientation. (a) Taft wave. (b) El centro wave. (c) Shanghai artificial wave.

**Table 3**

Comparison of maximum displacements at the location of measurement points between test and FE analysis results (mm).

Method	Height (m)	Sequency	FOE7				DBE7				MCE7			
			Input		2	3	4	5	6	7	9	10	11	13
			Excitation orientation		X	Y	X	Y	X	Y	X	X	X	X
Test	0.4	X direction	1.15	1.28	1.26	2.75	1.96	1.38	1.56	3.23	1.89	2.87	3.99	3.50
	2.5		4.24	3.35	4.42	5.98	4.79	4.07	11.31	12.44	12.44	24.31	26.97	26.93
	3.6		4.13	3.24	4.43	5.23	4.89	4.25	11.61	12.59	12.66	25.08	28.28	27.89
	0.4	Y direction	1.05	1.10	1.27	1.39	2.17	1.54	1.22	1.11	1.74	2.72	2.17	1.17
	2.5		2.31	3.38	3.67	3.18	3.75	4.34	6.86	10.82	9.47	14.94	23.96	20.29
	3.6		2.33	3.39	3.62	3.32	3.71	4.56	7.07	10.64	9.72	14.99	23.13	20.99
FE analysis	0.4	X direction	1.01	1.13	1.99		1.65	3.55	2.12		3.04	3.45	3.66	
	2.5		4.43	4.66	4.58		10.89	14.22	14.56		27.63	28.66	28.35	
	3.6		4.55	4.70	4.65		12.01	14.88	15.11		29.04	31.06	30.64	
	0.4	Y direction	0.90	1.12	2.11		1.11	1.32	2.01		2.51	2.61	1.25	
	2.5		2.12	3.42	3.80		6.26	9.65	8.99		12.66	20.85	23.55	
	3.6		2.50	3.49	3.88		6.78	9.98	9.64		13.19	21.56	25.39	
Test/FE analysis	0.4	X direction	1.14	1.12	0.98		0.95	0.91	0.89		0.94	1.16	0.96	
	2.5		0.96	0.95	1.05		1.04	0.87	0.85		0.88	0.94	0.95	
	3.6		0.91	0.94	1.05		0.97	0.85	0.84		0.86	0.91	0.91	
	0.4	Y direction	1.17	1.13	1.03		1.10	0.84	0.87		1.08	0.83	0.94	
	2.5		1.09	1.07	0.99		1.10	1.12	1.05		1.18	1.15	0.86	
	3.6		0.93	1.04	0.96		1.04	1.07	1.01		1.14	1.07	0.83	
Average			0.990											
Standard deviation			0.104											
Variation coefficient			0.106											

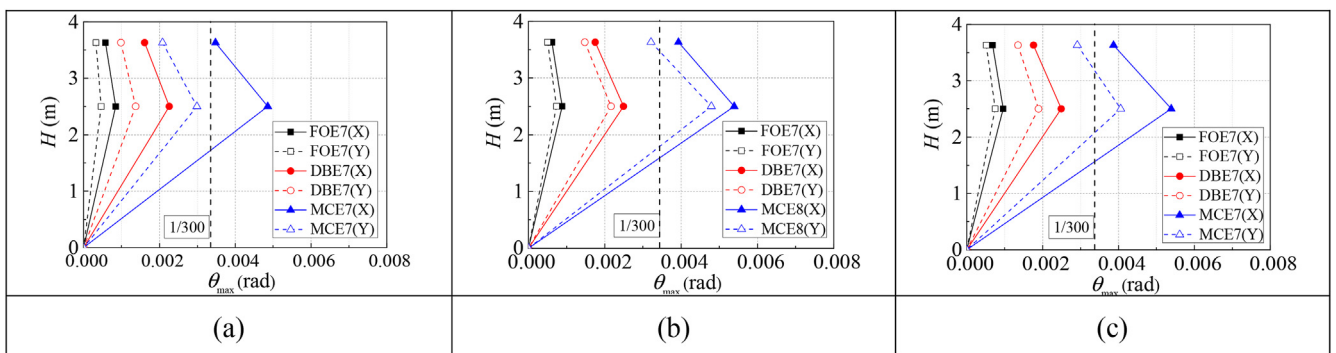


**Fig. 10.** Maximum story drift in X excitation orientation. (a) Taft wave. (b) El centro wave. (c) Shanghai artificial wave.

structural model was fastened to the model base through hold-down bolts and shear bolts, the corresponding displacement and rotations in  $x$ ,  $y$ , and  $z$  directions of the bottom face in the FE model

were restrained. The weight of CFS building was considered by defining the gravitational acceleration of  $9.8 \text{ m/s}^2$  in Y direction.

For the material of CFS components, von Mises yield criterion

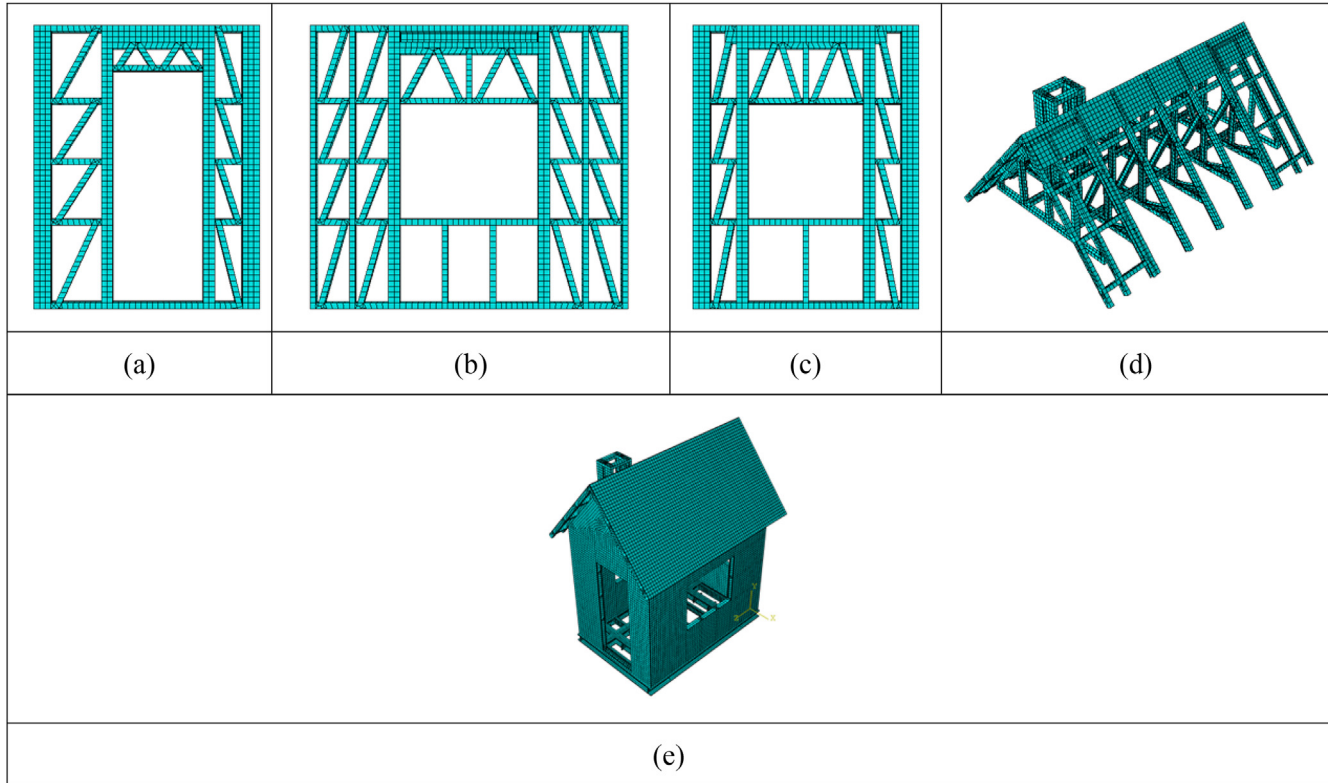


**Fig. 11.** FE model of the CFS building. (a) Shear wall L1. (b) Shear wall L2 and L4. (c) Shear wall L3. (d) Roof truss. (e) FE model.

was used with bilinear constitutive model, where the yield stress and ultimate tensile stress were 322.4 MPa and 477.73 MPa, respectively. The Poisson's ratio and elastic modulus of CFS components were 0.3 and  $2.08 \times 10^5$  MPa. The nonlinear combined hardening model was defined in the plastic behavior of CFS components along with the cyclic hardening for considering the Bauschinger effect of metal materials [41]. The material property of OSB sheathing was assumed orthotropy, where the flexure strength, elastic modulus, shear modulus and Poisson's ratio parallel to the longitudinal direction were 19.6 MPa, 3790 MPa, 944 MPa and 0.3, respectively; the flexure strength, elastic modulus, shear modulus and Poisson's ratio perpendicular to the longitudinal direction were 13.2 MPa, 1770 MPa, 962 MPa and 0.11, respectively. Under the action of FOE and DBE, the structural damping ratio was selected as 3%; while under the action of MCE, the structural damping ratio was selected as 5% [42].

The analysis results of developed FE model were validated against the results of shake table tests performed on the CFS building. Firstly, the modal analysis was carried out to obtain the frequencies and vibration modes of FE model in the first three order. Secondly, dynamic time-history analysis was conducted by referring to test working conditions in Table 1, and bidirectional seismic waves were applied to obtain the acceleration response and displacement response at the measuring points of FE model under the action of 7° earthquake. Table 4 shows the comparison of the frequencies based on test and FE analysis, and the corresponding first three vibration modes are shown in Fig. 12. The comparison of acceleration response and displacement response at the location of measurement points between test and FE analysis results are shown in Tables 2 and 3. It can be seen from three tables that the differences of the frequencies, maximum accelerations and displacements obtained from the shake table tests and analysed by FE analysis were both within 15%, indicating that the FE model can well simulate the mechanical behavior of CFS building under the

**Table 4**  
Comparison of the first two frequencies from test and FE analysis.

Mode shape	Vibration Direction	Test	FE	Test/FE
First order	Translation in Z direction	10.9	12.6	0.87
Second order	Translation in X direction	16.4	18.1	0.91
Third order	Torsion	—	25.3	—

action of 7° earthquake. The main reason for the error was that the loading condition of the test was continuous loading. Although the test phenomenon showed that the structure did not suffer obvious damage, the damage was still accumulating. However, the loading condition of FE model on dynamic time-history analysis was separate loading, so the difference in loading mode between the test and FE analysis influenced the results to some extent. In conclusion, The nonlinear FE modeling method was relatively reliable, and can be used for subsequent variable parameter analysis.

### 3.2. Parametric analysis

Based on the verified model of the CFS building, parametric investigation was conducted through eight FE models to determine the influence of subsequent various factors on the seismic behavior of CFS buildings. Details including sheathing panel material, diagonal bracing, story number, aspect ratio and plane layout were varied as shown in Table 5. It should be noted that the dimension in X direction of models is defined as its length  $L$ , the dimension in Z direction of models is defined as its width  $W$ , and the aspect ratio is the length-to-width ratio  $L/W$ . It can be known from the previous test results, the earthquake response of the CFS building under Shanghai artificial wave was the most visible. As a result, the shanghai artificial wave was selected in the parametric analysis for all FE models, and two different intensity levels including frequent

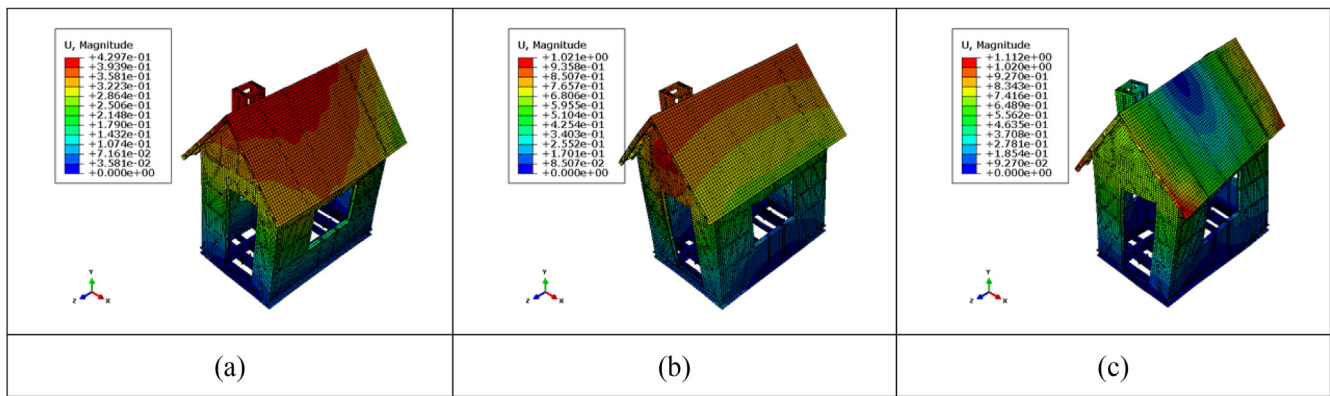


**Fig. 12.** Vibration shapes of FE model at first three orders. (a) First order. (b) Second order. (c) Third order.

occurring earthquake with a PGA of 0.07 g at intensity level 8° (FOE8) and maximum considered earthquake with a PGA of 0.400 g at intensity level 8° (MCE8) respectively were studied. The eight FE models with different structural shapes were shown in Fig. 13, and the FE modeling method was described above. It should be noted that the shear walls in Z direction of FE models was consistent with that in X direction of the test specimen, the shear walls in X direction of FE models was consistent with that in Y direction of the test specimen. The seismic response analysis was carried out in two steps. Referring to section 3.1, the modal analysis was the first step and dynamic time-history analysis was the second step. The working conditions of dynamic time-history analysis were shown in Table 6. Bidirectional seismic waves were applied to obtain the acceleration response and displacement response of FE models under the action of 8° earthquake, and Z direction was set as the main direction and the PGA in the X direction was proportioned by a factor of 0.85. The measuring points located in the bottom of shear wall, the top of shear wall and the top of roof truss. The fundamental frequencies and the maximum story drift of the CFS building models in parametric analysis were presented in Table 5.

### 3.2.1. Influence of the sheathing material

Comparing M1 with double-side 0.76 mm thick steel sheathing with Test with double-side 9.5 mm thick OSB sheathing, the fundamental frequency increased from 12.6 Hz to 13.0 Hz, representing a little impact on the dynamic characteristic with a 3.17% increase. Furthermore, the effect of sheathing material on the results of acceleration response and displacement response shown in Fig. 14. In the Z direction of the FE models, the maximum acceleration and displacement at the height of 3.6 m of M1 under FOE8 were 6.3% and 21.1% respectively smaller than that of Test, and under MCE8 were no and 9.5% respectively smaller than that of

Test. In the X direction of the FE models, the maximum acceleration and displacement at the height of 3.6 m of M1 under FOE8 were 9.6% and 20.3% respectively smaller than that of Test, and under MCE8 were 2.0% and 19.4% respectively smaller than that of Test. In addition, it was 1/622 and 1/776 for M1 under FOE8 in Z direction and X direction of the FE model respectively, which was less than 1/250. And similarly it was 1/212 and 1/264 for M1 under MCE8 in Z direction and X direction of the FE model respectively, which was less than 1/50. These results suggest that M1 with steel sheathing has better integral rigidity and seismic performance than Test with OSB sheathing due to the shear wall with steel sheathing has higher strength, bearing capacity and lateral stiffness than the shear wall with OSB sheathing.

The seismic performance of CFS building can be improved less than 20% by changing the material of shear wall sheathing. When OSB board is used as wall sheathing in engineering applications, its thickness should not be less than 9 mm according to the standard JGJ 227-2011 [32]; and when steel plate is used as wall sheathing, its thickness should not be less than 0.69 mm according to the standard JGJ/T 421-2018 [43].

### 3.2.2. Influence of the diagonal bracing

It can be known in Table 5 that the fundamental frequency of M2 without diagonal bracing was 10.2 Hz. Compared with Test with diagonal bracing, the positive effect of using diagonal bracing in shear walls resulted in a significant increase by 23.5% in the fundamental frequency. The lateral stiffness of shear wall with diagonal bracing get better. Furthermore, the acceleration amplification factor curves and story drift curves of FE model affected by setting diagonal bracing were observed in Fig. 15. In the Z direction of the FE models, the maximum acceleration and displacement at the height of 3.6 m of M2 under FOE8 were 17.1% and 15.0% higher than that of Test, respectively; and under MCE8 were 28.8% and

**Table 5**  
Structural parameters of FE models.

Specimen	Wall sheathing		Diagonal bracing	Story number	Span number (X direction)	Span number (Z direction)	Aspect ratio	f/Hz	$\theta_{\max}$
	Thickness /mm	Material						FOE8	MCE8
test	9.5	OSB	Yes	1	1	1	1.5	12.6	1/562 1/166
M1	0.76	Steel	Yes	1	1	1	1.5	13.0	1/622 1/212
M2	9.5	OSB	No	1	1	1	1.5	10.2	1/430 1/152
M3	9.5	OSB	Yes	2	1	1	1.5	7.6	1/382 1/150
M4	9.5	OSB	Yes	1	3	1	4.6	11.2	1/521 1/144
M5	9.5	OSB	Yes	1	3	2	2.3	12.8	1/658 1/192
M6	9.5	OSB	Yes	1	3	3	1.5	13.5	1/826 1/260
M7	9.5	OSB	Yes	2	3	3	H-shape	11.0	1/613 1/210
M8	9.5	OSB	Yes	2	3	3	U-shape	12.1	1/746 1/264

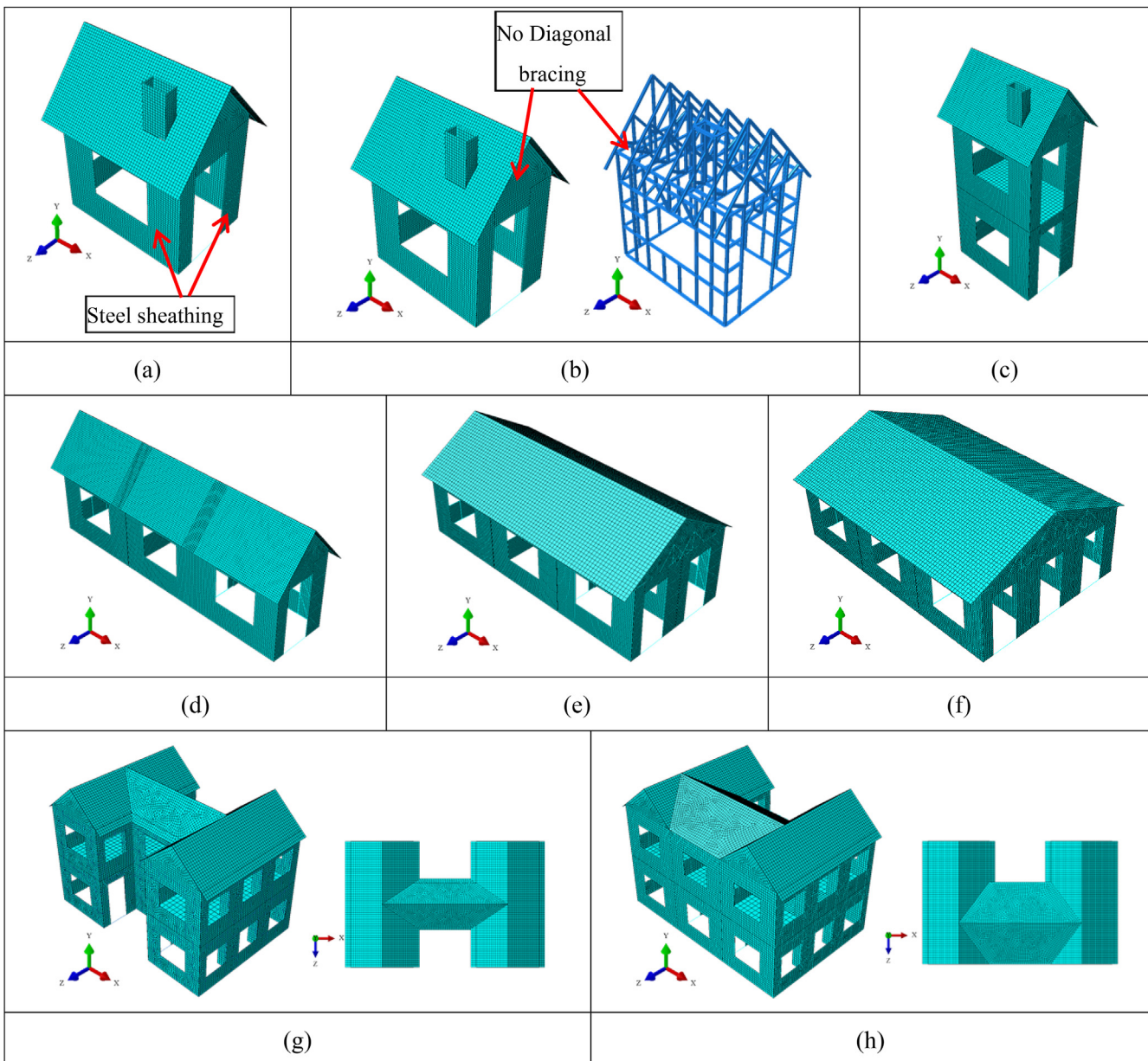


**Fig. 13.** Eight FE models in variable parameter analysis. (a) Specimen M1. (b) Specimen M2. (c) Specimen M3. (d) Specimen M4. (e) Specimen M5. (f) Specimen M6. (g) Specimen M7. (h) Specimen M8.

**Table 6**

Loading program in the variable parameter analysis.

Sequence	Level	Seismic wave	Excitation orientation	PGA/g	
				Z	X
1	FOE8	Shanghai artificial wave	Z	0.070	0.0595
2	MCE8			0.400	0.340

34.0% higher than that of Test, respectively. In the X direction of the FE models, the maximum acceleration and displacement at the height of 3.6 m of M2 under FOE8 were 11.4% and 9.3% higher than that of Test, respectively; and under MCE8 were 21.6% and 22.0% higher than that of Test, respectively. Moreover, it was 1/430 and 1/602 for M2 under FOE8 in Z direction and X direction of the FE model respectively, which was less than 1/250. And similarly it was 1/152 and 1/190 for M2 under MCE8 in Z direction and X direction of the FE model respectively, which was less than 1/50.

In conclusion, setting diagonal bracing in shear walls can significantly improve the dynamic characteristics and seismic performance of CFS building. As a result, the fundamental frequency of CFS building increases as well as the acceleration response and displacement response of CFS building reduced. The main reason is that the setting of diagonal bracing greatly improves the lateral stiffness of the shear wall, and then greatly improves the rigidity of the whole structure. It is suggested to set diagonal brace in shear walls of CFS building in the seismic fortification area of 8°.

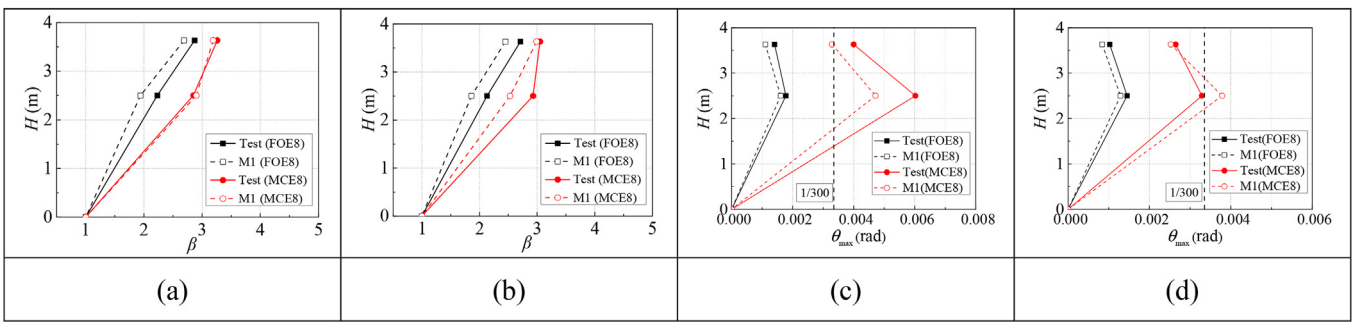


**Fig. 14.** Influence of sheathing material on acceleration response and displacement response. (a) Acceleration amplification factor curves in Z direction. (b) Acceleration amplification factor curves in X direction. (c) Story drift curves in Z direction. (d) Story drift curves in X direction.

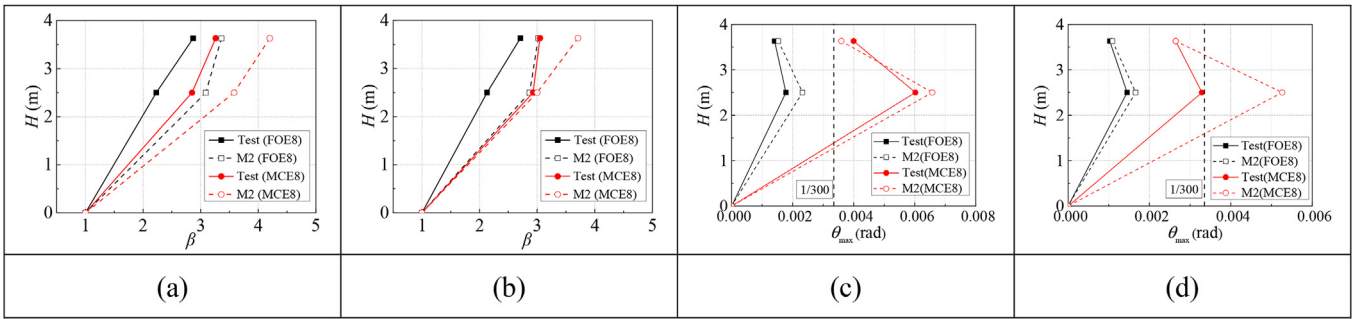


**Fig. 15.** Influence of diagonal bracing on acceleration response and displacement response. (a) Acceleration amplification factor curves in Z direction. (b) Acceleration amplification factor curves in X direction. (c) Story drift curves in Z direction. (d) Story drift curves in X direction.

### 3.2.3. Influence of the story number

Comparing M3 of two-layer CFS building with Test of single-layer CFS building, the fundamental frequency decreased from 12.6 Hz to 7.6 Hz, representing a obviously impact on the frequency with a 39.7% decrease. Furthermore, the effect of story number on the results of acceleration response and displacement response shown in Fig. 16. In the Z direction of the FE models, the maximum acceleration and displacement at the height of 2.5 m of M3 under FOE8 were 19.3% and 19.3% respectively higher than that of Test, and under MCE8 were 9.5% and 15.2% respectively higher than that of Test. In the X direction of the FE models, the maximum acceleration and displacement at the height of 2.5 m of M3 under FOE8 were 9.4% and 11.7% respectively higher than that of Test, and under MCE8 were 10.9% and 14.5% respectively higher than that of Test. In addition, it was 1/382 and 1/492 for M3 under FOE8 in Z direction and X direction of the FE model respectively, which was less than 1/250. And similarly it was 1/150 and 1/182 for M3 under MCE8 in Z direction and X direction of the FE model respectively, which was

less than 1/50.

The above analysis results show that the vibration frequency of CFS building is closely related to the height of the structure and decreases inversely with the increase of the height of the structure. The maximum acceleration and displacement at each measuring point of two-story FE model increases with the increase of the structural height, which is approximately proportional linear growth. The acceleration response and displacement response of CFS building increase with the number of floor story, and the seismic performance of the structure decreases. The weak position of CFS building does not change with the increase of floor story, and the maximum story drift of model M1 and model Test occur at the structural height of 2.5 m.

### 3.2.4. Influence of the aspect ratio

Comparing with M5 with the aspect ratio of 2.3 and M6 with the aspect ratio of 1.5, the fundamental frequency of M4 with the aspect ratio of 4.6 decreased 12.5% and 17.0% respectively. As the

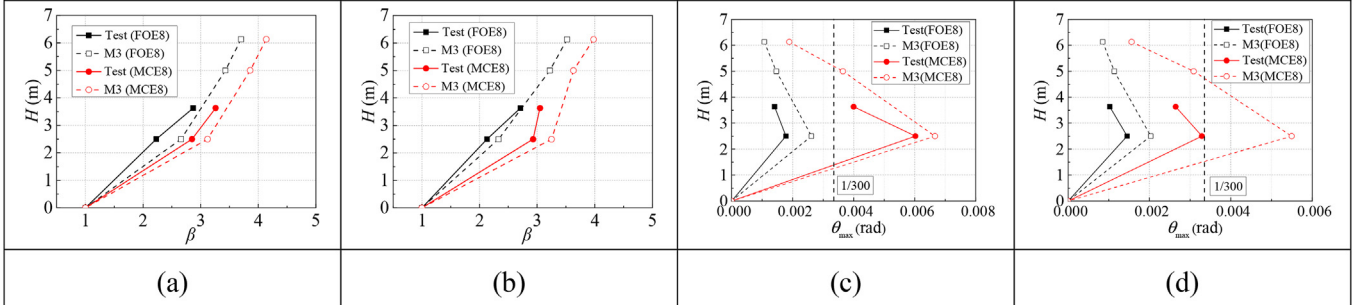


**Fig. 16.** Influence of story number on acceleration response and displacement response. (a) Acceleration amplification factor curves in Z direction. (b) Acceleration amplification factor curves in X direction. (c) Story drift curves in Z direction. (d) Story drift curves in X direction.

decrease of the aspect ratio, the vibration frequency of CFS building increased. Furthermore, the effect of aspect ratio on the results of acceleration response and displacement response shown in Fig. 17. In the Z direction of the FE models, the maximum acceleration at the height of 3.6 m of M4 under FOE8 were 32.4% and 56.9% higher than that of M5 and M6 respectively, and under MCE8 were 31.7% and 52.3% higher than that of M5 and M6 respectively. Moreover, the maximum displacement at the height of 3.6 m of M4 under FOE8 were 12.7% and 45.5% higher than that of M5 and M6 respectively, and under MCE8 were 14.0% and 30.1% higher than that of M5 and M6 respectively. In the X direction of the FE models, the maximum acceleration at the height of 3.6 m of M4 under FOE8 were 21.2% and 29.7% higher than that of M5 and M6 respectively, and under MCE8 were 21.9% and 28.0% higher than that of M5 and M6 respectively. Moreover, the maximum displacement at the height of 3.6 m of M4 under FOE8 were 10.3% and 18.5% respectively higher than that of M5 and M6, and under MCE8 were 10.7% and 23.5% higher than that of M5 and M6 respectively. In addition, it was 1/521 and 1/877 for M4 under FOE8 in Z direction and X direction of the FE model respectively, which was less than 1/250. And similarly it was 1/144 and 1/362 for M4 under MCE8 in Z direction and X direction of the FE model respectively, which was less than 1/50.

In summary, when the aspect ratio of CFS building decreases, that is, the plane shape of the building structure changes from narrow to regular, the overall rigidity and seismic performance of the structure increases. Therefore, the vibration frequency of CFS building increases as well as the acceleration response and displacement response of the structure decrease. In engineering design, the plan of the building shall be simple, regular and symmetrical. The structural layout shall be coordinated with the building layout, and the irregular plan shall not be adopted. The CFS shear wall shall be uniformly arranged in the building plane, which can be designed according to the plane structure in the two main axes.

### 3.2.5. Influence of the plane layout

The common square box building in practical projects had good seismic performance and engineering application background [44], but the layout of the building would be subject to the requirements of building site, urban planning, architectural art and use function. Some specific architectural plane shapes were inevitably used such as H-shape and U-shape. Based on this, the seismic performance of M7 with the plane layout of H-shape and M8 with the plane layout of U-shape under 8° earthquake were analysed.

The fundamental frequency of M7 and M8 were 11.0 Hz and 12.1 Hz respectively, which were slightly higher than the calculated value of formula JGJ 227-2011 [32] due to the lateral stiffness with inclined bracing in the shear walls higher than the structure used ordinary shear walls. The first and second order vibration modes of

the two FE models were translational mode, and the third order vibration mode was torsion mode, indicating that the vibration mode of CFS building with H-shape and U-shape were regular. Furthermore, the effect of plane layout on the results of acceleration response and displacement response shown in Fig. 18. In the Z direction of the FE models, the maximum acceleration and displacement at the height of 5 m of M7 under FOE8 were 12.5% and 16.4% higher than that of M8 respectively, and under MCE8 were 8.0% and 16.8% higher than that of M8 respectively. In the X direction of the FE models, the maximum acceleration and displacement at the height of 5 m of M7 under FOE8 were 3.7% and 9.3% higher than that of M8 respectively, and under MCE8 were 3.0% and 7.0% higher than that of M8 respectively. In addition, it was 1/613 and 1/980 for M7 under FOE8 in Z direction and X direction of the FE model respectively, which was less than 1/250. And similarly it was 1/210 and 1/442 for M7 under MCE8 in Z direction and X direction of the FE model respectively, which was less than 1/50.

The results of analysis indicate that the overall stiffness of H-shape building is smaller than that of U-shape building, and the difference of lateral stiffness in Z direction is more obvious. Therefore, the vibration frequency of U-shape building is larger, while the acceleration response and displacement response are lower than that of H-shape building. In conclusion, both CFS buildings show good seismic performance, which meet the seismic requirement of 8° seismic action.

## 4. Discussion and design recommendations

Although CFS structural buildings have good seismic performance, there is no systematic guiding design standard for recommending the aseismatic design and seismic construction measures of CFS structure in China. Therefore, the seismic construction measures of CFS structure are explored in this paper, which combined with the shaking table tests and the actual project cases.

### 4.1. Shear wall

Shear wall is the main resistance component to horizontal seismic force in CFS building. There are many factors influencing the seismic performance of shear wall, including the material of wall sheathing, diagonal bracing between columns, cross-section form of end column and lintel structure. Therefore, this article refer to the test results and FE analysis, from the following aspects of CFS structure to summarize the aseismatic structural measures.

(1) Shear walls with double-sided structural panels have better seismic performance. The thickness of OSB board and steel plate are larger than 9 mm and 0.69 mm respectively as wall sheathing in engineering applications. The minimum thickness of wood structural panel sheathing is the same as AISI

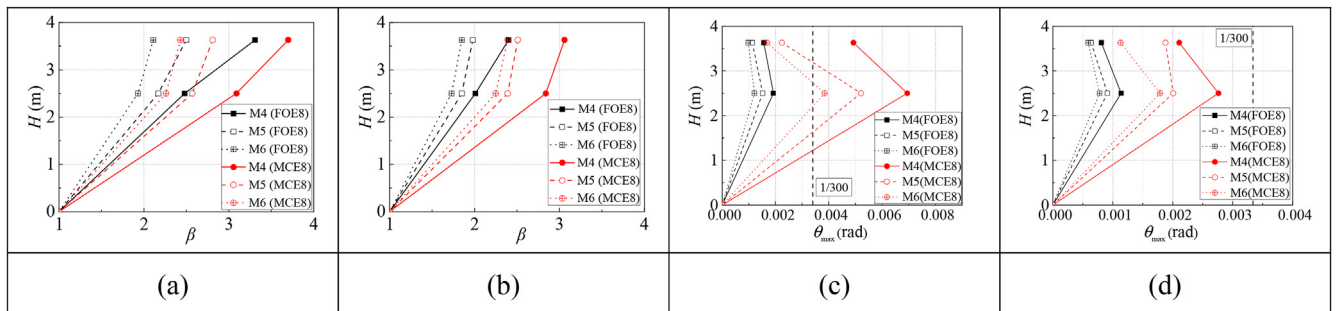


**Fig. 17.** Influence of aspect ratio on acceleration response and displacement response. (a) Acceleration amplification factor curves in Z direction. (b) Acceleration amplification factor curves in X direction. (c) Story drift curves in Z direction. (d) Story drift curves in X direction.

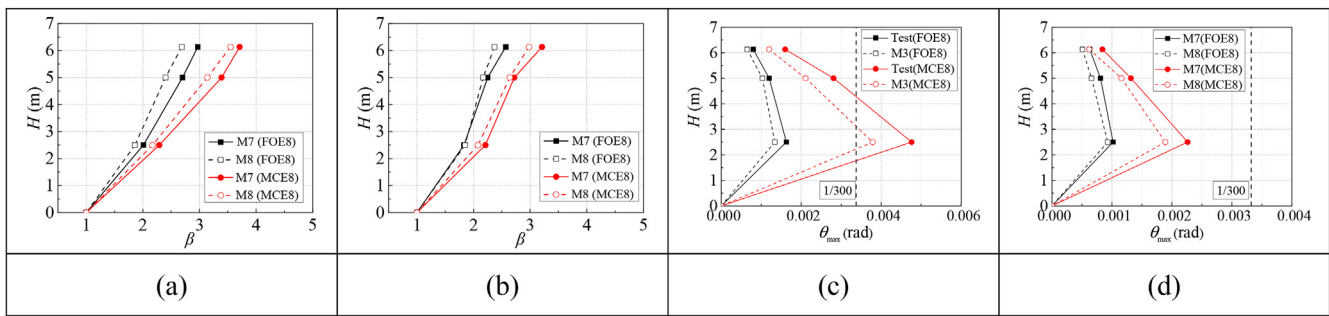


**Fig. 18.** Influence of plane layout on acceleration response and displacement response. (a) Acceleration amplification factor curves in Z direction. (b) Acceleration amplification factor curves in X direction. (c) Story drift curves in Z direction. (d) Story drift curves in X direction.

S400-15 [45], while the minimum thickness of steel sheet sheathing is more conservative than AISI S400-15 [45], due to the 0.46 mm-thick steel sheet sheathing can be used in CFS structural system in North American.

- (2) In the area with seismic fortification intensity greater than 8°, diagonal bracings should be set between the wall studs, whose section size is the same as the wall studs, and the thickness should not be less than 1 mm.
- (3) Overturning moment will occur to the shear wall under horizontal earthquake action, and the axial force generated by overturning moment is borne by the end stud of the wall. Therefore, according to the structural details of corner framing in AISI S230-15 [33], the multi-limbs built-up stud at the end of the wall is adopted to improve the vertical bearing capacity and seismic performance of the structure, as shown in Fig. 19. The connection strap is needed to connect each limb member of the built-up stud, and the spacing along the longitudinal direction of the stud shall not be greater than 300 mm as well as the size of the connection strap shall not be less than 50 mm × 1 mm.
- (4) For the shear wall with a big hole, the truss lintel above the hole needs to be strengthened to improve the bearing capacity and seismic performance. Hence, according to AISI S230-15 [33], an L-header shall consist of a CFS angle with one short leg lapping over the top track of the wall and one leg extending down the side of the wall above window or door openings. The L-header shall be placed on both sides of the wall opening to form double L-headers, as shown in Fig. 20. Each angle shall be fastened to top track above an opening with No.8 screws spaced at 305 mm on center. The vertical leg of the L-header shall be attached to at least one bearing stud at each end and each cripple stud with a

minimum No.8 screw at top and bottom. The top screw in the vertical leg of L-header shall be located not more than 25.4 mm from the top edge of the vertical leg. The minimum design thickness of L-header shall not be less than 0.84 mm.

#### 4.2. Roof truss

Roof sheathing should be laid on the roof trusses to transfer load and keep overall stability of the roof. Moreover, the ceiling joist top flange bracings, roof rafter bottom flange bracing and longitudinal vertical bracings should be placed in the roof trusses, as shown in Fig. 21.

- (1) Based on AISI S230-15 [33], U-shape, C-shape and Hat-shape CFS component or steel strip with the thickness more than 0.84 mm could be used as ceiling joist top flange bracing, where is fastened to the top flange of ceiling joist with one No.8 screw. Lateral bracing shall be installed perpendicular to the ceiling joists. Blocking shall be installed between joists in-line with bracing at a maximum spacing of 3.66 m measured perpendicular to the joist. Ends of lateral bracing shall be attached to blocking or anchored to a stable building component with No.8 screws. Furthermore, gypsum board

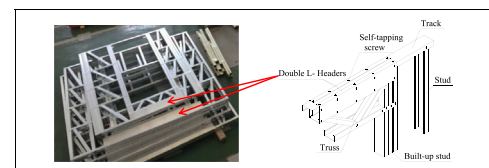


**Fig. 20.** Double L-headers in the lintel.

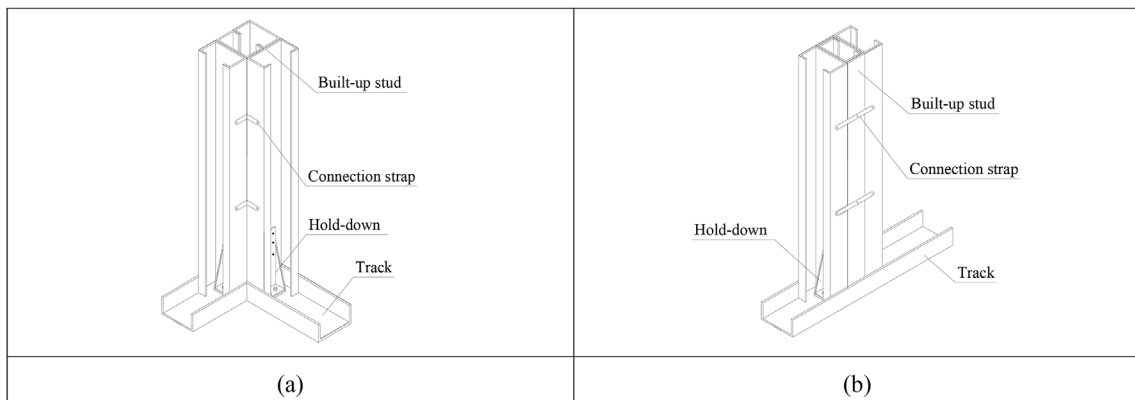


**Fig. 19.** The multi-limbs built-up stud at the end of the wall. (a) At the corner of the building. (b) In the middle of the building.

and steel strip with the spacing less than 1.2 m could be used as ceiling joist bottom flange bracing, where is fastened to the bottom flange of ceiling joist and perpendicular to the joist run. Blocking shall be installed between joists at a maximum spacing of 3.7 m measured along a line of continuous strapping.

- (2) Based on AISI S230-15 [33], U-shape and C-shape CFS component or steel strip with the thickness more than 0.84 mm could be used as roof rafter bottom flange bracing and longitudinal vertical bracing, where are fastened to the bottom flange of roof rafter and the middle web member of the roof trusses respectively. The bracing element shall be fastened to the bottom flange of each roof rafter with one No.8 screw and shall be fastened to blocking with two No.8 screws. Blocking shall be installed between roof rafters inline with the continuous bracing at a maximum spacing of 3.66 m measured perpendicular to the roof rafters.
- (3) In order to enhance the overall stiffness and collaborative performance of roof trusses, it is suggested to set full-length L-shape connector at the roof ridge connected to roof rafters by two No.8 screws spaced at 305 mm on center, as shown in Fig. 21. The thickness of L-shape connector shall not be less than 0.84 mm according to AISI S240-15 [46].

#### 4.3. Architectural layout

In order to meet the requirements of seismic design, the building layout shall be simple, regular and symmetrical. The ratio of length to width of the building should not be too large to avoid the use of long and narrow structural form. Because the irregular vibration mode produced by the ground motion phase difference under the action of the earthquake make two sides of the structure are not consistent with vibration, which lead to earthquake damage. Therefore, the long and narrow structural form should be avoided in the structural plane layout. Moreover, AISI S400-15 [45] specifies the aspect ratio (length: width) of the diaphragm sheathed with wood structural panels should not exceed 4:1 for blocked diaphragms and 3:1 for unblocked diaphragms.

For H-shape building and U-shape building with irregular concave and convex plan, the extension length of the building plane should be as small as possible so as to ensure the great in-plane stiffness of the floor slab and prevent the structural vibration of different parts from being out of sync. Local earthquake damage is easily caused when the local overhang size is larger than 30% of the total size at the corresponding projection direction. In addition, the design requirement of diaphragms in open front structures is specified in AISI S400-15 [45] that the length of the diaphragm normal to the open side cannot exceed 7.62 m, and the aspect ratio (length: width) is less than 1: 1 for one-story structures or 2: 3 for structures over one story in height, where the length dimension of the diaphragm is perpendicular to the opening. Hence, if the local overhang size exceeds the limit, it is suggested to use commercial software for seismic analysis of the whole structure. Meanwhile,

strengthened measures need to be adopted at the concave corner in the structural design.

#### 5. Conclusion

Based on the shaking table test and FE analysis, the seismic performance of a single-storey prefabricated CFS building was studied. The primary conclusions are summarized as follows:

- (1) Under 7° frequent, basic and rare earthquake action, the prefabricated CFS building showed good seismic performance. The structural weakness such as the holes of windows and doors, and main lateral force resisting member such as CFS frame and wall sheathing had not obvious damage phenomenon. The whole stiffness and natural frequency of CFS structure had no obvious changes. The CFS structure was still in the elastic stage after 7° earthquake. The fundamental frequency result of CFS building is consistent with the calculation results of JGJ 277-2011. The maximum story drift of CFS building meet the requirement of deformation limit of JGJ 277-2011 and GB 50011-2010. The pre-fabricated CFS building meet the seismic fortification requirements of “small earthquake is not bad, medium earthquake can be repaired, major earthquake does not fall”. Moreover, the CFS building has a large safety reserve of seismic action.
- (2) It is suggested that the damping ratio of CFS building should be 3% under the action of FOE and DBE as well as the damping ratio of CFS building should be 5% under the action of MCE.
- (3) In areas of high fortification intensity, the CFS frame with double-sided steel plates and diagonal bracings are recommended to use for improving seismic performance. It is suggested to adopt smaller aspect ratio as well as simple, regular and symmetrical plane layout of CFS building.
- (4) In order to improve the seismic design method of CFS structure, the seismic construction measures of CFS structure are discussed in this paper from the three aspects of shear wall, roof truss and architectural layout.

#### Conflicts of interest

The authors declared that they have no conflicts of interest to this work.

We declare that we do not have any commercial or associative interest that represents a conflict of interest in connection with the work submitted.

#### Acknowledgments

The authors wish to acknowledge the support of the “Natural Science Foundation of China” funded by National Natural Science Foundation of China (51908047 and 51890902), the Natural Science Basic Research Plan in Shaanxi Province of China (2018JQ5037), and Fundamental Research Funds for the Central Universities, CHD (300102289112). Any opinions, findings, and conclusions or recommendations expressed in this paper are those of the authors and do not necessarily reflect the views of the sponsors.

#### References

- [1] W. Khaliq, A. Moghis, Shear capacity of cold-formed light-gauge steel framed shear-wall panels with fiber cement board sheathing, *Int. J. Steel Struct.* 17 (4) (2017) 1404–1414.
- [2] J.P. Hao, B. Liu, D.Y. Hao, et al., Test on shear resistance of cold-formed thin-walled X-shaped steel strap-braced framing walls with sprayed lightweight



**Fig. 21.** Measures for aseismic structure of roof truss.

- mortar. *J. Build. Struct.* 35 (12) (2014) 20–28 (in Chinese).
- [3] W. Chen, J.H. Ye, Y. Xu, Shear experiments of load-bearing cold-formed thin-walled steel wall system lined with sandwich panels, *J. Build. Struct.* 38 (7) (2017) 85–92 (in Chinese).
- [4] Y.Q. Li, C. Hong, Y.F. Qin, Experimental study on shear performance of CCA-sheathed light-gauge steel framing walls, *J. Build. Struct.* 36 (9) (2015) 151–157 (in Chinese).
- [5] Y.H. Wang, R. Deng, X.M. Yao, et al., Experiment on seismic behavior of cold-formed thin-walled steel walls with diagonal braces, *J. Architect. Civil Eng.* 36 (2) (2019) 30–38.
- [6] Y. Shi, X.H. Zhou, S.F. Nie, et al., Research on the seismic performance of cold-formed steel stud wall, *China Civ. Eng. J.* 43 (s1) (2010) 124–129 (in Chinese).
- [7] L.F. Guo, Shear Behavior of Light-Gauge Steel Stud Walls in Residential Buildings, Doctoral dissertation, Xi'an University of Architecture and technology, Xi'an, China (in Chinese).
- [8] L.A. Fülop, D. Dubina, Performance of wall-stud cold-formed shear panels under monotonic and cyclic loading: Part I: experimental research, *Thin-Walled Struct.* 42 (2) (2004) 321–338.
- [9] K.D. Peterman, B.W. Schafer, Sheathed cold-formed steel studs under axial and lateral load, *J. Struct. Eng.* 140 (10) (2014), 04014074-1(12).
- [10] W.Y. Zhang, M. Mahdavian, Y.Q. Li, et al., Experiments and simulations of cold-formed steel wall assemblies using corrugated steel sheathing subjected to shear and gravity loads, *J. Struct. Eng.* 143 (3) (2016), 04016193.
- [11] Y. Noritsugu, Y. Cheng, Effective strip method for the design of cold-formed steel framed shear wall with steel sheet sheathing, *J. Struct. Eng.* 140 (4) (2014), 04013101.
- [12] A. Hoseinpoor, T.M.R. Javaheri, Cyclic loading tests for cold-formed steel wall frames with lightweight concrete, *Civ. Eng. Infrastruct. J.* 50 (1) (2017) 119–133.
- [13] O. Pourabdollah, F. Farahbod, F.R. Rofooei, The seismic performance of K-braced cold-formed steel shear panels with improved connections, *J. Constr. Steel Res.* 135 (2017) 56–68.
- [14] A. Sato, C.M. Uang, A FEMA P695 study for the proposed seismic performance factors for cold-formed steel special bolted moment frames, *Earthq. Spectra* 29 (1) (2013) 259–282.
- [15] L. Fiorino, S. Shakeel, V. Macillo, R. Landolfo, Behaviour factor ( $\alpha$ ) evaluation of the CFS braced structures according to FEMA P695, *J. Constr. Steel Res.* 138 (2017) 324–339.
- [16] S. Shakeel, R. Landolfo, L. Fiorino, Behaviour factor evaluation of CFS shear walls with gypsum board sheathing according to FEMA P695 for Eurocodes, *Thin-Walled Struct.* 141 (2019) 194–207.
- [17] Y. Qi, M.Z. Su, L.L. Zhang, et al., Shaking table test and finite element analysis of low-rise cold-formed thin-walled steel residential buildings, *J. Architect. Civil Eng.* 26 (3) (2009) 71–75 (in Chinese).
- [18] Z.G. Huang, M.Z. Su, B.K. He, et al., Shaking table test on seismic behaviors of three-story cold-formed thin-walled steel residential buildings, *China Civ. Eng. J.* 44 (2) (2011) 72–81 (in Chinese).
- [19] Y.Q. Li, F. Liu, Z.Y. Shen, et al., Shaking table test of two full-scale models of S350 cold-formed thin-walled steel framing buildings, *China Civ. Eng. J.* 45 (10) (2012) 135–144 (in Chinese).
- [20] Y.Q. Li, Z.Y. Shen, X.Y. Yao, et al., Experimental investigation and design method research on low-rise cold-formed thin-walled steel framing buildings, *J. Struct. Eng.* 139 (5) (2013) 818–836.
- [21] K.D. Peterman, M.J.J. Stehman, S.G. Buonopane, et al., Seismic Performance of Full-Scale Cold-Formed Steel Buildings, Tenth U.S. National Conference on Earthquake Engineering, Anchorage, Alaska, 2014.
- [22] K.D. Peterman, M.J.J. Stehman, R.L. Madsen, et al., Experimental seismic response of a full-scale cold-formed steel-framed building. I: system-level response, *J. Struct. Eng.* 142 (12) (2016), 04016127.
- [23] K.D. Peterman, M.J.J. Stehman, R.L. Madsen, et al., Experimental seismic response of a full-scale cold-formed steel-framed building. II: subsystem-level response, *J. Struct. Eng.* 142 (12) (2016), 04016128.
- [24] B.W. Schafer, D. Ayhan, J. Leng, et al., Seismic response and engineering of cold-formed steel framed buildings, *Structure* 8 (2016) 197–212.
- [25] T.C. Hutchinson, X. Wang, G. Hegemier, et al., Physical Damage Evolution during Earthquake and Post-earthquake Fire Testing of a Mid-rise Cold-Formed Steel Framed Building, Eleventh U.S. National Conference on Earthquake Engineering, Los Angeles, California, 2018.
- [26] X. Wang, T.C. Hutchinson, G. Hegemier, et al., Earthquake and Fire Performance of a Mid-rise Cold-Formed Steel Framed Building – Test Program and Test Results: Rapid Release Report, University of California, La Jolla, California, 2016.
- [27] L. Fiorino, V. Macillo, R. Landolfo, Shake table tests of a full-scale two-story sheathing-braced cold-formed steel building, *Eng. Struct.* 151 (2017) 633–647.
- [28] J.H. Ye, L.Q. Jiang, Simplified analytical model and shaking table test validation for seismic analysis of mid-rise cold-formed steel composite shear wall building, *Sustainability* 10 (9) (2018) 3188.
- [29] L. Fiorino, B. Bucciero, R. Landolfo, Shake table tests of three storey cold-formed steel structures with strap-braced walls, *Bull. Earthq. Eng.* 17 (2019) 4217–4245.
- [30] Y.H. Wang, R. Deng, X.M. Yao, et al., Experiment on seismic behavior of cold-formed thin-walled steel walls with diagonal braces, *J. Architect. Civil Eng.* 36 (2) (2019) 30–38.
- [31] Y. Shi, X.H. Zhou, L.P. Liu, et al., Shaking table test on prefabricated light steel structure popular science building, *J. Build. Struct.* 40 (2) (2019) 98–107 (in Chinese).
- [32] MHURD, Technical Specification for Low-Rise Cold-Formed Thin Walled Steel Buildings, JGJ 227-2011, Ministry of Housing and Urban-Rural Development, Beijing, China, 2011 (in Chinese).
- [33] AISI, Standard for Cold-Formed Steel Framing -Prescriptive Method for One and Two Family Dwellings, AISI S230-15, American Iron and Steel Institute, Washington, DC, USA, 2015.
- [34] GAQSIQ and SAC, Metallic Materials-Tensile Testing-Part 1: Method of Test at Room Temperature, GB/T 228.1-2010, General Administration of Quality Supervision, Inspection and Quarantine of P.R. China, Standardization Administration of P.R. China, Beijing, China, 2011 (in Chinese).
- [35] X.H. Zhou, Y. Shi, L. Xu, et al., A simplified method to evaluate the flexural capacity of lightweight cold-formed steel floor system with oriented strand board subfloor, *Thin-Walled Struct.* 134 (2019) 40–51.
- [36] GAQSIQ and SAC, Load Code for the Design of Building Structures, GB 50009-2012, General Administration of Quality Supervision, Inspection and Quarantine of P.R. China, Standardization Administration of P.R. China, Beijing, China, 2012 (in Chinese).
- [37] GAQSIQ and SAC, Code for Seismic Design of Buildings, GB 50011-2010, General Administration of Quality Supervision, Inspection and Quarantine of P.R. China, Standardization Administration of P.R. China, Beijing, China, 2010 (in Chinese).
- [38] ASCE, Minimum Design Loads and Associated Criteria for Buildings and Other Structures, ASCE/SEI 7-16, American Society of Civil Engineers, Structural Engineering Institute, Reston, VA, 2016.
- [39] ABAQUS Inc., Abaqus. (6.13, Computer-aided engineering, Finite Element Analysis Pawtucket, USA, 2013.
- [40] GAQSIQ and SAC, Standard for Design of Steel Structures, GB 50017-2017, General Administration of Quality Supervision, Inspection and Quarantine of P.R. China, Standardization Administration of P.R. China, Beijing, China, 2017 (in Chinese).
- [41] Q.X. Shi, F. Wang, P. Wang, et al., Experimental and numerical study of the seismic performance of an all-steel assembled Q195 low-yield buckling-restrained brace, *Eng. Struct.* 176 (1) (2018) 481–499.
- [42] R.K. Ma, Y.Q. Li, FEA on seismic behavior of low-rise cold-formed thin-walled steel framing buildings, *J. Build. Struct.* 35 (5) (2014) 40–47 (in Chinese).
- [43] MHURD, Technical Standard for Cold-Formed Thin-Walled Steel Multi-Storey Residential Buildings, JGJ/T 421-2018, Ministry of Housing and Urban-Rural Development, Beijing, China, 2018 (in Chinese).
- [44] X.H. Zhou, Y. Guan, Y. Shi, Seismic performance analysis of multi-story cold-formed thin-walled steel structure residential buildings, *Progress Steel Build. Struct.* 19 (6) (2017) 10–50 (in Chinese).
- [45] AISI, North American Standard for Seismic Design of Cold-Formed Steel Structural Systems, AISI S400-15, American Iron and Steel Institute, Washington, DC, USA, 2015.
- [46] AISI, North American Standard for Cold-Formed Steel Structural Framing, AISI S240-15, American Iron and Steel Institute, Washington, DC, USA, 2015.